


Article

Interval Type-2 Fuzzy Dynamic High Type Control of Permanent Magnet Synchronous Motor with Vector Decoupling Method

Xinglong Chen ^{1,2}, Wei Tong ³, Yao Mao ^{1,2,*}  and Tao Zhao ³

¹ Key Laboratory of Optical Engineering, Chinese Academy of Sciences, Chengdu 610209, China; chenxinglong@ioe.ac.cn

² Institute of Optics and Electronics, Chinese Academy of Sciences, Chengdu 610209, China

³ College of Electrical Engineering, Sichuan University, Chengdu 610065, China; tongwei@stu.scu.edu.cn (W.T.); zhaotaozhaogang@scu.edu.cn (T.Z.)

* Correspondence: maoyao@ioe.ac.cn; Tel.: +86-135-4787-8788

Abstract: This paper presents an interval type-2 fuzzy dynamic high type (IT2FDHT) control based on vector decoupling method for permanent magnet synchronous motor (PMSM) to improve the dynamic characteristics of the system. Firstly, to address the shortcomings of the traditional PI regulator used in the current loop of PMSM, an improved PI regulator based on voltage feed-forward decoupling is used. Then, considering the characteristics that the higher the system type, the smaller the steady-state error and the shorter the regulation time, the high type control structure is added. However, a purely high type structure amplifies the oscillations of the system and is extremely sensitive to perturbations, which can easily lead to system divergence. Therefore, in order to solve the problems caused by high type structure, finally we designed dynamic high type control with the help of fuzzy logic systems (FLSs), which successfully achieved automatic switching of system type while improving response speed and steady-state accuracy. Meanwhile, quantum-behaved particle swarm optimization (QPSO) algorithm is employed to determine the parameters of FLSs. In summary, five methods including conventional PI, feed-forward decoupling PI (FDPI), FDPI high type (FDPI-HT), FDPI type-1 fuzzy dynamic high type (FDPI-T1FDHT), and FDPI-IT2FDHT, are compared to show the superiority of the proposed method. By means of simulations, the excellence of proposed FDPI-IT2FDHT is verified.



Citation: Chen, X.; Tong, W.; Mao, Y.; Zhao, T. Interval Type-2 Fuzzy Dynamic High Type Control of Permanent Magnet Synchronous Motor with Vector Decoupling Method. *Actuators* **2021**, *10*, 293. <https://doi.org/10.3390/act10110293>

Academic Editor: Shuxiang Dong

Received: 13 September 2021

Accepted: 29 October 2021

Published: 2 November 2021

Publisher's Note: MDPI stays neutral with regard to jurisdictional claims in published maps and institutional affiliations.



Copyright: © 2021 by the authors. Licensee MDPI, Basel, Switzerland. This article is an open access article distributed under the terms and conditions of the Creative Commons Attribution (CC BY) license (<https://creativecommons.org/licenses/by/4.0/>).

Keywords: dynamic high type; fuzzy logic systems; permanent magnet synchronous motor; feed-forward decoupling

1. Introduction

The advantages of PMSM are small size, simple structure, light weight, low losses. It does not have commutator and brushes of DC motor, and it is characterized by high efficiency, high power factor, large torque inertia ratio, small current and resistance losses, high reliability and strong coupling [1–3]. One of the more widely used control methods for these motors is the vector control method with rotor field orientation. The basic principle of operation is to decouple the magnetic field current and torque current of the motor on a synchronous coordinate system with rotor field orientation through coordinate transformation, so that it has the same operating performance as the conventional DC motor [4–6]. The vector control system of PMSM can realize high precision, high dynamic performance, and wide range of speed regulation or positioning control, so the vector control system of PMSM has attracted a lot of attention from scholars at home and abroad [7–9].

However, vector control only achieves the static decoupling of the two current components, not the dynamic decoupling, and the coupling voltage exists in the dynamic process, especially at high speed, the coupling voltage can even reach 30% of the stator

voltage [10], causing the two current components to affect each other, which makes the control performance of the system reduced. Dynamic decoupling is the compensation of coupling voltage to improve the control performance of the servo system based on the static decoupling. Here, feed-forward decoupling is used to compensate for the coupling voltage. By means of feed-forward decoupling, [11] used a predictive current control method to improve the dynamic performance of the system, but the method is strongly influenced by the motor parameters and is not robust. Ref. [12] applied a neural network decoupling control method, which required a large amount of experimental sample data for offline training and was relatively complicated to implement. Therefore, it is necessary to find a robust and easy-to-implement method, and high type control is such a method that meets the requirements.

High type control [13] mainly refers to the parallel connection of one or more integrators in the forward path of the system to increase the system type and thus improve some aspect of the system performance. The integrator is an electronic component commonly used in control circuits, whose output signal is the time product of the input signal. From the physical point of view, it can convert acceleration signal into velocity signal and velocity signal into position signal, which is an essential device in the multi-closed loop system. According to the principle of automatic control, the greater the number of integrators in the forward path of a closed-loop control system, the higher the system type [14]. Commonly used multi-closed-loop control systems are generally Type I or Type II systems. The higher the type, the smaller the steady-state error and the shorter the regulation time, but the system oscillation is also larger and extremely sensitive to disturbances, which can easily lead to system divergence [13]. In order to overcome the instability of the high type system and retain its advantages of high accuracy, researchers have tried different approaches. Tang constructed a PID-I type system by adding an integrator to the PID controller to take advantage of the large closed-loop bandwidth of the PID so that the high-type system can accommodate more disturbances [15]. Papadopoulos et al. designed an explicit analytical PID tuning rule for Type III control loop design based on the symmetric optimality criterion [16]. However, this static way of increasing the system type has the pitfall that the integral saturation may occur when there is a large or high frequency sudden change in the system input, which may prevent the actuator from working properly. To solve the problem of integral saturation in high type systems, dynamic high type techniques using FLSs are proposed, adaptively turning on or off the integrator according to the system status to achieve dynamic switching type, which can improve the tracking performance of the system while avoiding the saturation of the integrator.

FLSs have an excellent ability in dealing with various uncertainties and interferences [17–19]. At present, FLSs are mainly divided into type-1 FLSs (T1FLSs) and type-2 FLSs (T2FLSs). T1FLSs achieve a successful application in the area of fuzzy control because of its simple structure and convenient calculation. As the complexity and performance requirements of the control system increase, T1FLSs become increasingly inadequate to meet the control needs. Thus, T2FLSs, especially interval T2FLSs (IT2FLSs), have come into the limelight and are gradually being used in various fields [20–22]. In IT2FLSs, the pros and cons of the membership parameters and the related parameters of the controller are directly reflected in the control effect. Especially for the nonlinear controlled system with high complexity and high precision, traditional parameter setting methods are often difficult to meet control requirements. In addition, because the dimension and complexity of IT2FLSs are higher than those of traditional T1FLSs, it is difficult for conventional optimization methods to obtain effective parameter configuration. Intelligent optimization algorithms [23–25], as very popular methods in recent years, have been applied extensively for solving global optimization problems.

QPSO [25] is an intelligent optimization algorithm based on conventional PSO idea. PSO [24] was proposed on the basis of studies on the predatory behavior of birds. Although PSO has a wide range of applications, compared with QPSO, PSO has more parameters such as inertia weight w , acceleration coefficient c and scope of search space V_{max} to be

set, which is not conducive to finding the global optimal solution, and for some complex nonlinear systems, the lack of randomness in particle position changes makes it easy to fall into the dilemma of local optimization. Combined quantum mechanics and PSO, QPSO improves on the shortcomings of PSO. Regarding the quantum behavior of a particle, its motion state can be described according to the quantum uncertainty principle and the global optimal solution is found throughout the feasible solution space. Therefore, QPSO is a strategy with better global convergence than PSO. Here, we employed QPSO to determine optimal parameters of FLSs.

In conclusion, in this article, based on feed-forward decoupling PI, an IT2FDHT control method using QPSO is proposed to improve dynamic performance of PMSM. The main contributions of this paper are briefly summarized as follows:

- (1) Fuzzy dynamic high type methods are provided for the vector decoupling control of PMSM.
- (2) Aiming at the problem that related parameters in the IT2FLSs are difficult to determine, QPSO is employed.
- (3) In addition to the proposed method, PI, FDPI, FDPI-HT, FDPI-T1FDHT are also designed for simulations.

The remainder of the paper is structured as follows. Section 2 introduces PMSM mathematical model and vector control in summary. Considering PMSM traditional control methods, conventional PI and FDPI are provided in Section 3. Next, in Section 4, we will focus on fuzzy dynamic high type methods for PMSM control. Then, in Section 5, simulation analyses regarding PMSM are performed to demonstrate the excellence of FDPI-IT2FDHT method. Finally, Section 6 provides the conclusion as well as future work.

2. PMSM Mathematical Model and Vector Control

In this section, the PMSM mathematical model is introduced first, then the most commonly used vector control method is succinctly reviewed.

2.1. PMSM Mathematical Model

The PMSM is a multivariable coupled system. In order to realize the decoupling of the mathematical model of the PMSM, the mathematical model under d-q coordinates is normally used, which is convenient to analyze the steady-state and dynamic performance of the PMSM. So, when building a mathematical model of a PMSM, it is usually necessary to ignore some parameters that have little influence on the building of the mathematical model to simplify the analysis, and the following assumptions are generally made [26]:

- (1) Neglecting the saturation of the motor core;
- (2) Excluding eddy current and hysteresis losses in the motor;
- (3) The current in the motor is a symmetrical three-phase sine wave current.

Under the above conditions, the mathematical model of PMSM in a two-phase rotating coordinate system (d-q) can be obtained as

$$u_d = R_s i_d + \frac{d\psi_d}{dt} - \omega_r \psi_q \quad (1)$$

$$u_q = R_s i_q + \frac{d\psi_q}{dt} + \omega_r \psi_d \quad (2)$$

$$\psi_d = \psi_f + L_d i_d \quad (3)$$

$$\psi_q = L_q i_q \quad (4)$$

$$T_e = \frac{3}{2} p_n [\psi_f i_q + (L_d - L_q) i_d i_q] \quad (5)$$

where u_d , u_q , i_d , i_q , L_d , L_q , ψ_d , and ψ_q are the stator voltage, current, inductance, and flux linkage in the d-q coordinate system, respectively; R_s is the stator resistance; ψ_f is the

permanent flux linkage; w_r is the rotor electric angular velocity; p_n is the pole pairs; T_e is the electromagnetic torque.

Substituting the stator flux linkage Equations (3) and (4) into the stator voltage Equations (1) and (2)

$$\begin{cases} u_d = R_s i_d + L_d \frac{di_d}{dt} - w_r L_q i_q \\ u_q = R_s i_q + L_q \frac{di_q}{dt} + w_r (L_d i_d + \psi_f) \end{cases} \quad (6)$$

As can be seen from Equation (6), the stator inductance parameter causes cross-coupling in the d-q axis, and the larger the w_r is the stronger the coupling effect, and its influence is greater in the variable speed and high speed regions.

2.2. PMSM Vector Control

From the mathematical model of the PMSM, it is clear that the control of the electromagnetic torque can ultimately be reduced to the control of the d-axis current and the q-axis current, with constant system parameters. For a given output torque, there are many different combinations of d-axis current (excitation current) and q-axis current (torque current), and the different combinations will affect the system efficiency, power factor, motor terminal voltage and torque output capability, thus forming the current control strategy problem of the PMSM. Usually, the control strategy of $i_d = 0$ is adopted in the PMSM vector control system. The control method of $i_d = 0$ is relatively simple, the electromagnetic torque and i_q are linear, there is no direct axis armature reaction, no demagnetization effect, all current of the motor is used to generate electromagnetic torque, and the current control efficiency is high [27].

The structure of the PMSM vector control system is given in Figure 1. The system adopts a double closed-loop control structure with an internal current loop and an external speed loop. The position information detected by the position sensor is converted into the motor speed and compared with the reference speed to get the deviation number. This deviation signal is passed through the speed PI regulator to obtain the current torque component reference i_{qref} , and the stator current excitation component i_{dref} . The stator three-phase currents i_a, i_b, i_c measured by the phase current detection circuit are converted to i_d, i_q in the d-q coordinate system as the current loop feedback quantity through coordinate transformation.

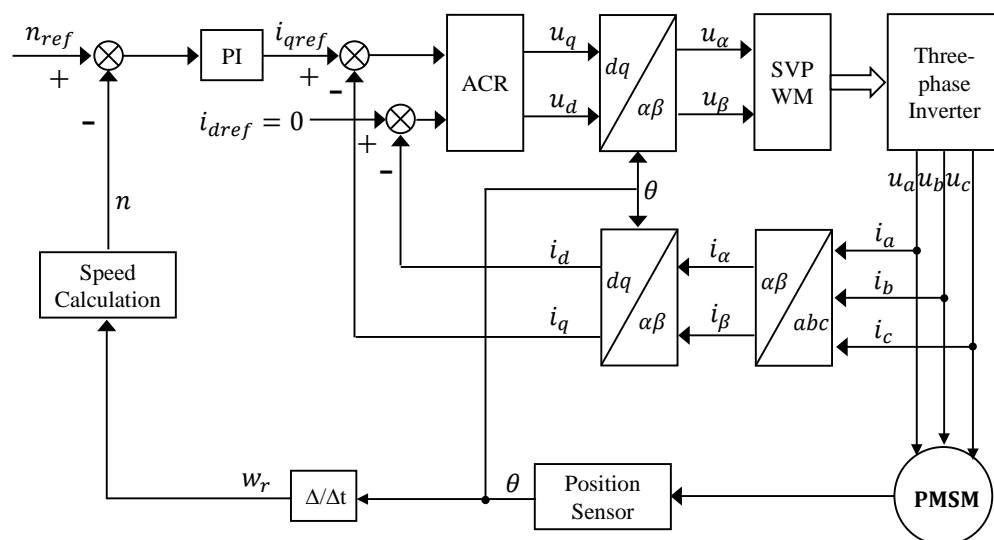


Figure 1. Structure of the PMSM vector control system.

The deviation signals obtained by comparing i_{dref}, i_{qref} with i_d, i_q are passed through the automatic current regulator (ACR) to obtain the voltage signals u_d, u_q in the d-q coord-

ordinate system. The voltage signals in the two-phase stationary coordinate system u_α, u_β are obtained by the Park inverse transformation and fed into the SVPWM algorithm to generate control pulses, which are used to control the switching state of the three-phase inverter and thus obtain the actual current of the three-phase symmetric winding of the control stator. In this control system, the outer speed loop generates the reference value of the stator current torque component and the inner current loop gets the actual control signal, thus forming a complete speed-current double closed-loop control system.

3. PMSM Traditional Control Methods

In this section, two classic approaches, namely PI and FDPI, are presented for the design of ACR.

3.1. Conventional PI

The conventional current control scheme uses two PI regulators for independent control of the d-q axis current. Here, the current regulator design of i_q channel is used as an example, and the current closed-loop control block diagram is shown in Figure 2.

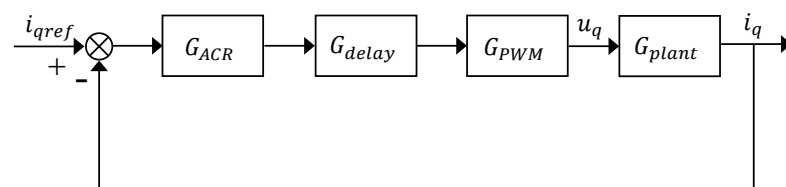


Figure 2. Current closed-loop control block diagram.

The first link in Figure 2 is the PI regulator, the second is the delay model, the third is the PWM model, and the fourth is the control object PMSM model. Their transfer functions can be expressed as follows, respectively.

$$G_{ACR} = K_p + \frac{K_i}{s} \tag{7}$$

$$G_{delay} = \frac{1}{T_s s + 1} \tag{8}$$

$$G_{PWM} = \frac{K_{PWM}}{0.5T_s s + 1} \tag{9}$$

$$G_{plant} = \frac{i_q}{u_q} = \frac{1}{L_q s + R_s} \tag{10}$$

where K_p, K_i are the coefficients of the PI regulator, T_s is the current sampling filter time constant, K_{PWM} is the amplification of PWM, L_q is the stator inductance and R_s is the stator resistance. Due to the high sampling frequency of the current, the delay link and the PWM link can be combined and processed, and then after letting $K_{PWM} = 1$ we can get

$$G_{delay} \cdot G_{PWM} = \frac{1}{0.5T_s^2 s^2 + 1.5T_s s + 1} \approx \frac{1}{1.5T_s s + 1} \tag{11}$$

At this point, the current loop in Figure 2 is adjusted according to a typical type-1 system [28], the open-loop transfer function is

$$G_{open} = \frac{K_p(\tau s + 1)}{\tau s} \frac{1}{R_s(\frac{L_q}{R_s}s + 1)} \frac{1}{1.5T_s s + 1} = \frac{K}{s(Ts + 1)} \tag{12}$$

If we make $\tau = \frac{L_q}{R_s}$, we can obtain the rectified open-loop transfer function

$$G_{open} = \frac{K_p}{R_s \tau s (1.5T_s + 1)} = \frac{K}{s(T_s + 1)} \quad (13)$$

Solving for K and T according to Equation (13)

$$K = \frac{K_p}{R_s \tau} = \frac{K_p}{L_q} \quad (14)$$

$$T = 1.5T_s \quad (15)$$

In order to make the current loop have fast response without large overshoot, it is designed as a typical type-1 system according to the engineering design method, and the damping factor is taken as 0.707, then $KT = 0.5$, and thus the coefficients of the PI regulator can be found [28].

$$K_p = \frac{L_q}{3T_s} \quad (16)$$

$$K_i = \frac{K_p}{\tau} = \frac{K_p R_s}{L_q} = \frac{R_s}{3T_s} \quad (17)$$

Considering the actual speed regulation system power supply rated voltage, rated current and other constraints, it is necessary to choose an anti-integration saturation PI regulator that limits the output quantity of the regulator and the internal integrator. The conventional PI current regulator is simple in structure and easy to implement, but ignores the influence of the d-q axis cross-coupling and only does the steady-state approximation coupling. The effect of the cross-coupling term is speed-dependent, and the coupling effect is significant during the speed regulation or in the high-speed section, which cannot meet the performance requirements by relying only on the PI regulator for current regulation.

3.2. Feed-Forward Decoupling PI

From Equation (6), it can be seen that there is a coupling term in the state equation when a conventional PI regulator is used. Part of the output voltage of the conventional PI regulator is used to offset the counter-electromotive force. Part of it is used to control the cross-direct axis current, which increases the regulation time and reduces the regulation accuracy and the dynamic performance of the system [29]. Therefore, by compensating the coupling term in Equation (18) in the conventional current regulator, the dynamic performance of the system can be improved.

$$\begin{cases} u_d' = u_d + w_r L_q i_q \\ u_q' = u_q - w_r L_d i_d - w_r \psi_f \end{cases} \quad (18)$$

Substituting Equation (18) into Equation (6) yields

$$\begin{cases} u_d' = R_s i_d + L_d \frac{di_d}{dt} \\ u_q' = R_s i_q + L_q \frac{di_q}{dt} \end{cases} \quad (19)$$

According to the above equation, it can be seen that there is no coupling in the voltage equation after compensation. Figure 3 shows the structure of the voltage feed-forward decoupled compensated current regulator design.

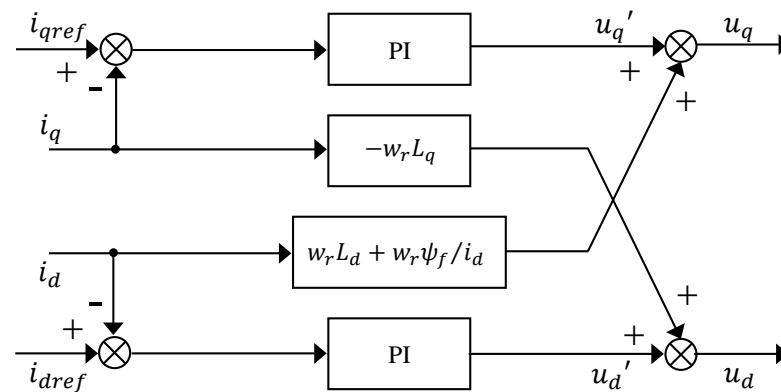


Figure 3. Structure of the voltage feed-forward decoupling PI.

4. Fuzzy Dynamic High Type Methods

In this section, firstly, we will present a detailed introduction of the QPSO algorithm. Then, the focus is the design of high type (HT) and fuzzy dynamic high type (T1FDHT and IT2FDHT).

4.1. QPSO Algorithm

For an N -dimensional optimization problem, we assume that there are M particles, and the position of each particle can represent a potential solution. In the t th generation of the particle population, the N -dimensional position of the i th particle can be represented as $X_i(t) = (X_{i,1}(t), X_{i,2}(t), \dots, X_{i,N}(t))$. Besides, the optimal positions of the i th particle and the particle population are denoted as $P_i(t) = (P_{i,1}(t), P_{i,2}(t), \dots, P_{i,N}(t))$ and $G(t) = (G_1(t), G_2(t), \dots, G_N(t))$, respectively. $P_i(t)$ is determined by the following equation

$$P_i(t) = \begin{cases} X_i(t), & f(X_i(t)) < f(P_i(t-1)) \\ P_i(t-1), & f(X_i(t)) \geq f(P_i(t-1)) \end{cases} \quad (20)$$

where the function $f(\cdot)$ is the fitness function, and $G(t)$ is calculated by Equation (21)

$$G(t) = P_g(t) \\ g = \arg \min_{1 \leq i \leq M} \{f(P_i(t))\} \quad (21)$$

Since the position and velocity of a particle cannot be determined simultaneously in quantum space, by means of the wave function we can describe the quantum state of the particle. Finally, the improved expressions for the particle position are obtained by the Monte Carlo method

$$p_{i,j}(t) = G_j(t) + \varphi \cdot (P_{i,j}(t) - G_j(t)) \quad (22)$$

$$X_{i,j}(t+1) = p_{i,j}(t) \pm \alpha \cdot |m_j(t) - X_{i,j}(t)| \cdot \ln(1/u) \quad (23)$$

where α is the contraction-expansion coefficient, u as well as φ are random numbers between 0 and 1, and the mean optimal position $m(t)$ is

$$m(t) = (m_1(t), m_2(t), \dots, m_N(t)) = \frac{1}{M} \sum_{i=1}^M P_i(t) \quad (24)$$

4.2. High Type

As mentioned in introduction, high type control is mainly a structure that improves the performance of a system in some way by adding one or more integrators to the forward path of the system. Figure 4 illustrates the structure of high type based on feed-forward decoupling PI, where e is speed error and k_u is the amplification factor of speed error.

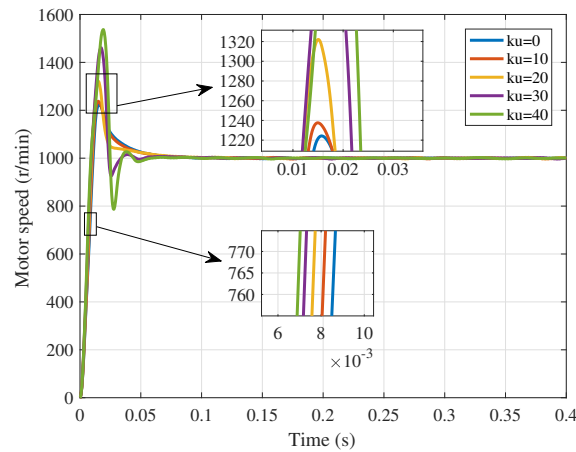


Figure 5. Comparison of HT control effect.

Table 1. Comparison of HT control indicators.

k_u	$t_r(10^{-3}s)$	$t_s(10^{-3}s)$	$\sigma\%$
0	7.4876	38.20	22.4%
10	7.0199	35.82	23.7%
20	6.5607	24.84	32.2%
30	6.1593	27.90	46.1%
40	5.8526	32.27	53.7%

4.3. Type-1 Fuzzy Dynamic High Type

Since the high type structure alone can lead to oscillation and even divergence problems, the dynamic high type technique was proposed. However, most of the related researches simply control the integrator on or off, and do not realize the standard of automatic switching type. In addition, the jitter caused by the switching instant is also difficult to eliminate. In the context of modernization, high demands are placed on the degree of automation and performance of PMSM, and the development of intelligent control technologies brings new possibilities for this purpose. Fuzzy logic, as one of the widely used intelligent control technologies, in combination with high type control structures, allows for automated dynamic high type control.

As can be seen from Figure 6, a T1FLS usually consists of four parts: fuzzifier, inference engine, rule base, and defuzzifier. First, the measurement inputs are processed by the fuzzifier to obtain type-1 fuzzy sets (T1FSs), and these T1FSs are mapped to all membership functions (MFs) to calculate the corresponding membership degrees. Next, the inference engine further determines the firing strengths of the rules based on the predefined rules in its rule base. After determining the membership degrees and firing strengths, the T1FSs can be calculated. Finally, a defuzzifier is used to process the output T1FSs to acquire the output of the system.

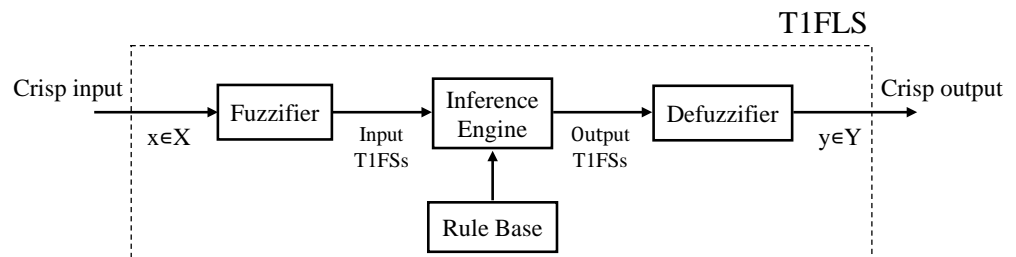


Figure 6. Structure diagram of a T1FLS.

The FLS is implemented by monitoring the error and error change. So, the inputs of the FLS, i.e., E and EC , can be of the form

$$E(k) = k_e \cdot e(k)$$

$$EC(k) = k_{ec} \cdot [e(k) - e(k - 1)]$$
(25)

where k is the sampling moment, k_e and k_{ec} are the scale coefficients of the two inputs.

So, the structure of the fuzzy dynamic high type (FDHT) based on feed-forward decoupling PI is designed in Figure 7.

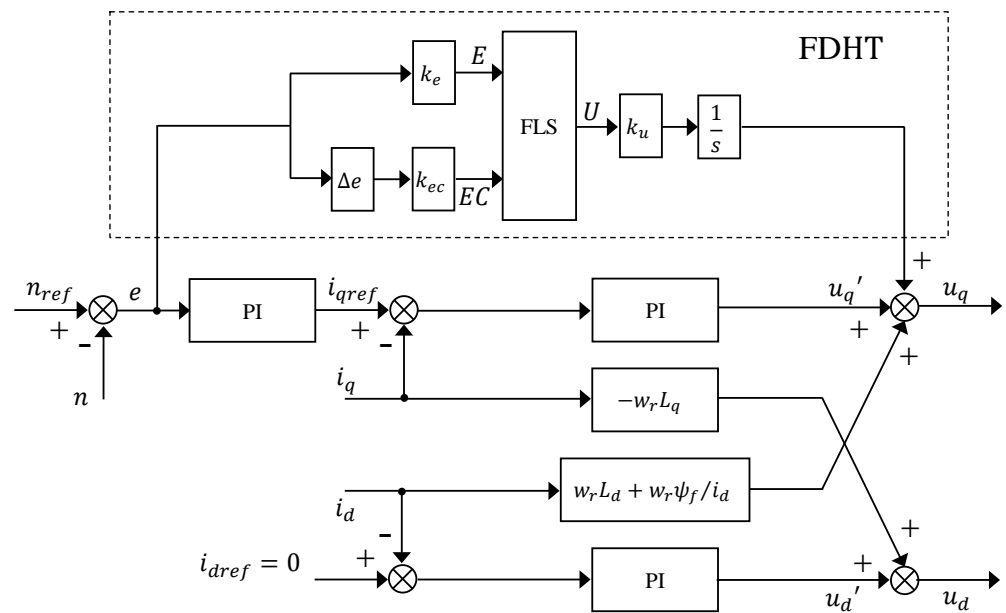


Figure 7. Structure of FDHT based on feed-forward decoupling PI.

Where Δe is the error change, U is the output of the FLS, and k_u is the amplification factor of the output. By using the FLS, the oscillation problem caused by the high type structure can be handled and the dynamic switching of system types can be realized.

Here, we mainly describe the design of T1FLS. Figure 8a,b, respectively, display MFs of input variable E and EC , and Figure 8c shows MFs of output variable U .

According to Figure 8, the T-S T1FLS with two inputs and a single output has a total of 15 rules, and the i -th rule has the following form

$$R^i : \text{IF } E \text{ is } M^i \text{ and } EC \text{ is } N^i \text{ THEN } U \text{ is } Y^i$$

where Y^i is the consequent, M^i and N^i are the antecedents of the i th rule.

Through some simulations and analysis, it is found that when the output of the FLS and the error have the same sign, it will strengthen the current trend of error variation, and vice versa will weaken this trend. Thus, if EC is N , when E is negative (NB or N), the amount of error will be increasing and we need to suppress this tendency, so the output of the FLS takes positive (P or PB), with the error difference sign. If EC is N , the amount of error gets smaller when E is positive (PB or P), and this trend needs to be accelerated, but we find that the traditional FDPI method produces overshoot, and to avoid overshoot, the output is taken as P or Z . Similarly, to reduce overshoot or oscillation, the output of the FLS is Z or N when E is Z . For the sense of brevity, only the case where EC is N is described. Table 2 lists the specific fuzzy rules of the T-S T1FLS.

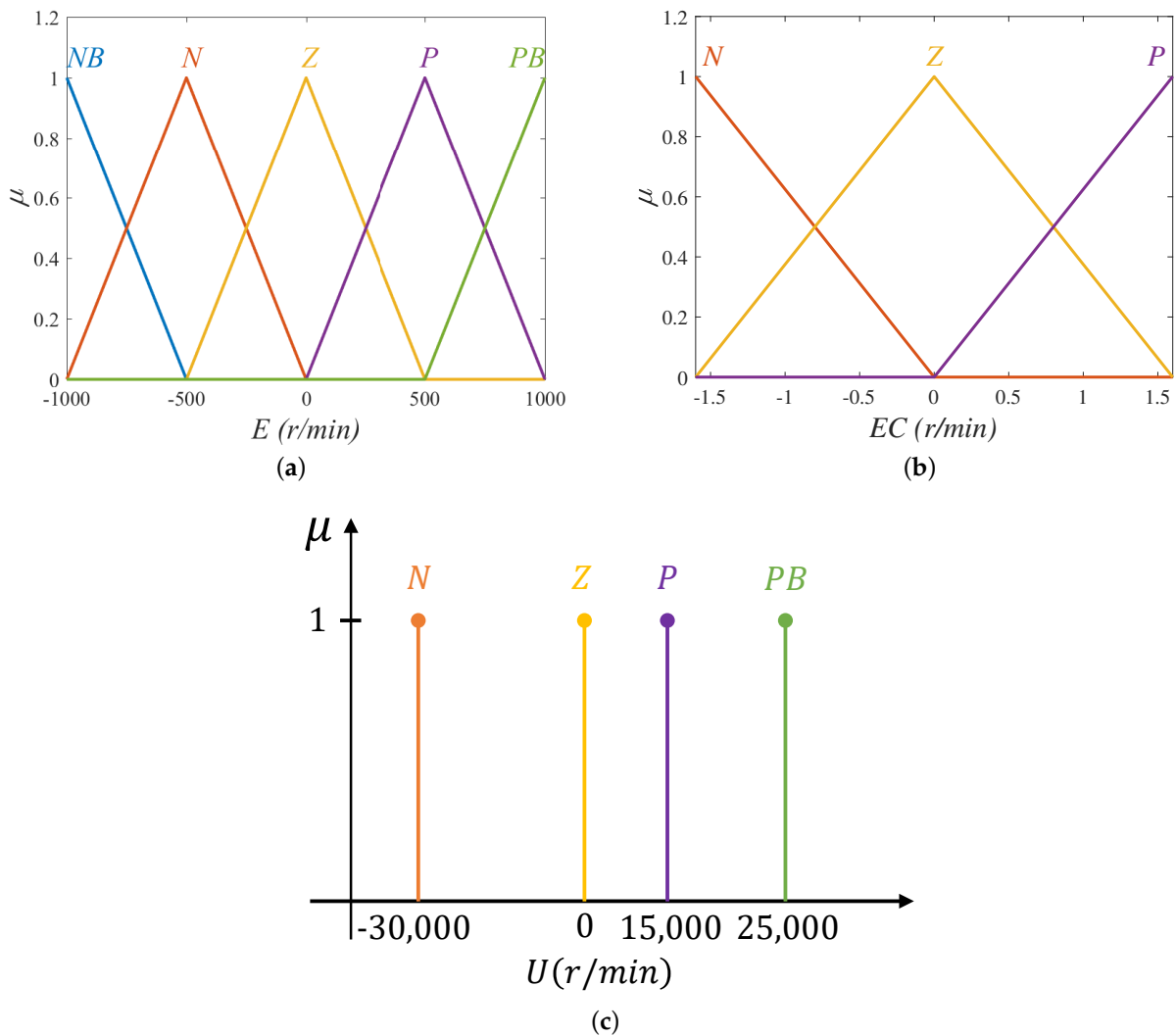


Figure 8. MFs of input and output variables. (a) MFs of input variable E ; (b) MFs of input variable EC ; (c) MFs of output variable U .

Table 2. T-S fuzzy rules of the system.

Rules		E				
		NB	N	Z	P	PB
EC	N	PB	PB	N	Z	P
	Z	P	Z	Z	PB	PB
	P	N	N	Z	N	N

By means of T1FLS, the T1FDHT based on FDPI, i.e., FDPI-T1FDHT, not only has a faster dynamic response, but can also handle a wide range of loads and perturbations. Nevertheless, faced with higher performance requirements and more load devices of PMSM, FDPI-T1FDHT is hardly perfect for the job.

4.4. Interval Type-2 Fuzzy Dynamic High Type

Figure 9 is the structure diagram of an IT2FLS. Compared with T1FLS in Figure 6, the main difference is that IT2FLS has an additional step of type-reduction. The role of type-reduction is to transform the T2FSs into T1FSs. Here, we use the common type-reduction inference approach, namely center-of-set (COS) type-reduction [30], to acquire T1FSs.

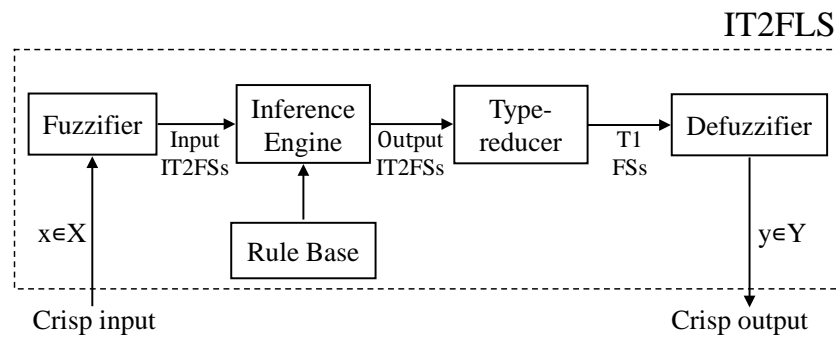


Figure 9. Structure diagram of an IT2FLS.

The input to the IT2FLS has the same form as the input to the T1FLS in Equation (25), and the only difference is the MFs of the input and output. Figure 10a,b present MFs of input variable E and EC in the IT2FLS, respectively. Table 3 shows consequent MFs of output variable U in the IT2FLS.

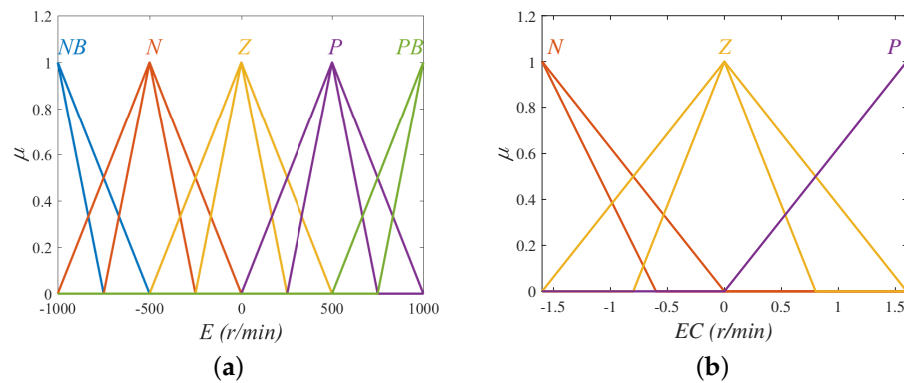


Figure 10. MFs of input variables in the IT2FLS. (a) MFs of input variable E ; (b) MFs of input variable EC .

Table 3. The consequent MFs of output variable U in the IT2FLS.

Consequent	Range (r/min)	Consequent	Range (r/min)
N	$[-35,000, -30,000]$	P	$[15,000, 20,000]$
Z	$[-10, 10]$	PB	$[25,000, 30,000]$

Regarding the rules, IT2FLS and T1FLS have the same design, as shown in Table 2. Eventually, we provide the structure of the PMSM vector control system applying FDPI-FDHT (FDPI-T1FDHT and FDPI-IT2FDHT) methods. The dashed box at the top of Figure 11 describes the design of FDHT, while the dashed box at the bottom of the Figure 11 shows the structure of the classic PI current regulator. f_1 and f_2 are the voltage feed-forward coupling compensation terms analyzed earlier. T_s and T_n are, respectively, the current sampling filter time constant and the speed sampling filter time constant [31].

Although the IT2FLS has better performance than T1FLS, the superiority of IT2FLS cannot be guaranteed if the appropriate parameters are not taken. Therefore, the relevant parameters (k_e, k_{ec}, k_u) of the IT2FLS are optimized by the QPSO algorithm introduced earlier, while the same optimization process is adopted for the T1FLS for the sake of the reasonableness of the comparison. In the next section, we will demonstrate the excellence of FDPI-FDHT, especially FDPI-IT2FDHT, through simulation analyses.

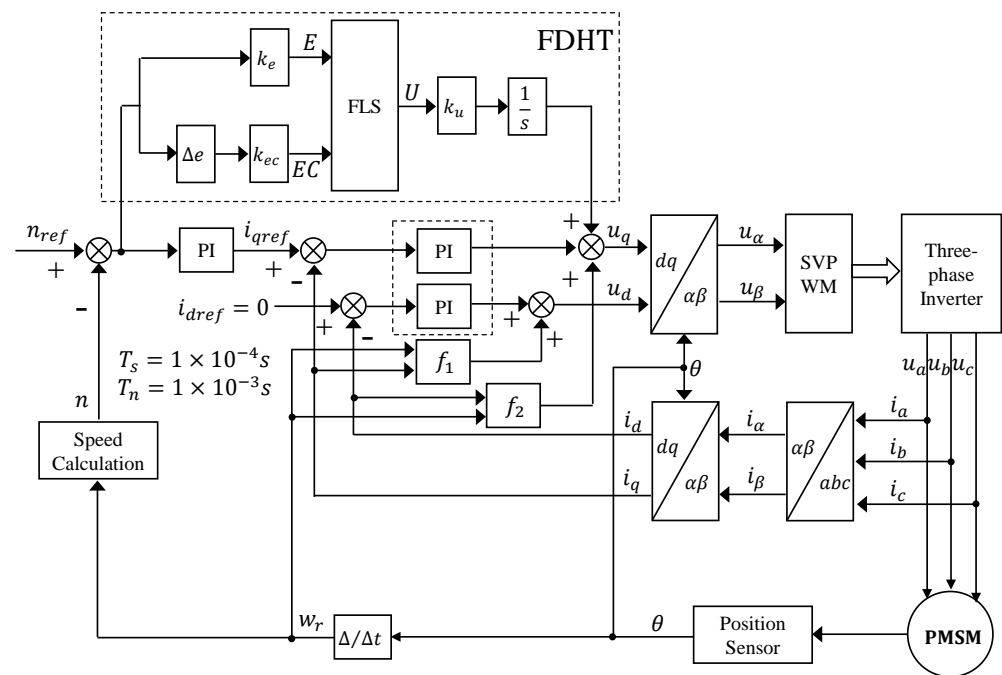


Figure 11. Structure of the PMSM vector control system applying FDPI-FDHT.

5. Simulation Analyses

In this section, comparative simulation experiments are implemented to verify the performance of the proposed FDPI-IT2FDHT method under no-load and load conditions of the PMSM. First, the QPSO algorithm is used to optimize the relevant parameters with the motor at no load to obtain the performance comparison in that case. Then, the motor is given a proper load and then the performance change under load is tested. Finally, the analyses of the two cases is used to show the superiority of the method in this paper.

5.1. Experimental Preparation

Table 4 lists the main parameters of the PMSM, and Table 5 shows the values of parameters of the three PI controllers. To ensure that the input of the FLS, i.e., the error change, is reasonable, a discrete system is used for the analysis, where the sampling period of the system is 10^{-4} s and the total simulation time is 0.4 s.

Table 4. Parameters of the PMSM.

Parameter	Value
Pole pairs p_n	4
Inertia $J/(\text{kg} \cdot \text{m}^2)$	0.003
Stator resistance R_s/Ω	0.958
d-axis inductance L_d/mH	5.25
q-axis inductance L_q/mH	12
Flux linkage ψ_f/Wb	0.1827
Viscous damping $F/(\text{N} \cdot \text{m} \cdot \text{s})$	0.008
Torque constant $k_T/(\text{N} \cdot \text{m} \cdot \text{A}^{-1})$	1.0962

Table 5. Parameters of the three PI controllers.

Parameter	Value
Speed outer loop K_p	0.14
Speed outer loop K_i	7
d-axis current inner loop K_p	17.5
d-axis current inner loop K_i	3193.3
q-axis current inner loop K_p	40
q-axis current inner loop K_i	3193.3

Next, the QPSO algorithm is used to optimize the relevant parameters in FDPI-HT, FDPI-T1FDHT, and FDPI-IT2FDHT methods. After comparing Figures 4 and 7, we find the high type control structure requires optimization of only one parameter (k_u), while the FDHT requires optimization of three parameters (k_e, k_{ec}, k_u). So, Table 6 lists the specific parameters used in QPSO algorithm.

Table 6. Parameters used in QPSO algorithm.

Parameter	Value
Maximum generation G	100
Population size M	50
Dimension N	1 or 3
Contraction-expansion coefficient α	[2, ..., 1]

In this table, N is the dimension, indicating the number of optimization parameters, and α is a contraction-expansion coefficient, which decreases linearly from 2 to 1. The choice of the fitness function in the optimization algorithm directly affects the effect of the algorithm, so the commonly used integral of absolute error (IAE) is used as the fitness function of the QPSO algorithm.

$$\text{IAE} = \int_0^{\infty} |e(t)| dt \quad (26)$$

To better show the prominence of the FDPI-IT2FDHT method, evaluation indicators are used to quantify the control performance of various methods. In addition to the IAE as the fitness function, the evaluation indicators also include integral of square error (ISE) and integral of time square error (ITSE).

$$\text{ISE} = \int_0^{\infty} |e(t)|^2 dt \quad (27)$$

$$\text{ITSE} = \int_0^{\infty} t|e(t)|^2 dt \quad (28)$$

The smaller the evaluation indicators, the better the method performance. Thus, according to the above analyses, we can acquire optimization results of FDPI-HT, FDPI-T1FDHT, and FDPI-IT2FDHT methods under no-load situation in Table 7.

Table 7. Optimization results of three methods under no-load situation.

Method	Optimized Parameters
FDPI-HT	$k_u = 24.3158$
FDPI-T1FDHT	$k_e = 1.0639, k_{ec} = 1.1092, k_u = 2.1819$
FDPI-IT2FDHT	$k_e = 0.5888, k_{ec} = 0.7088, k_u = 4.1344$

5.2. No-Load Situation

Under no-load condition, the motor speed is set to 1000 r/min and the performance of the five methods is compared. Figure 12 and Table 8, respectively, illustrate the motor speed tracking results and corresponding evaluation indicator results under no-load situation.

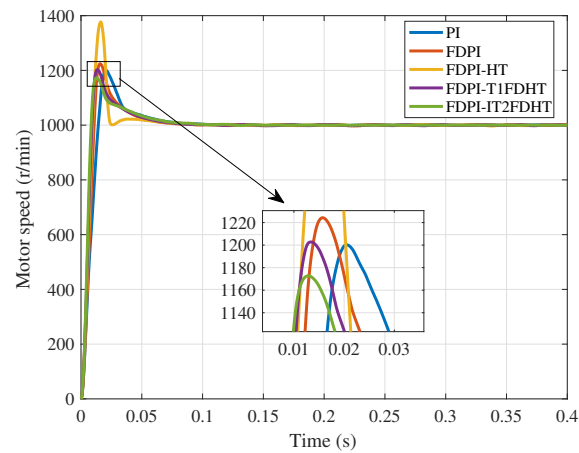


Figure 12. Motor speed tracking results under no-load situation.

Table 8. Evaluation indicator results under no-load situation.

Method	IAE	ITSE	ISE
PI	11.5138	28.8293	5.4714×10^3
FDPI	10.5075	23.4418	5.0137×10^3
FDPI-HT	9.8549	26.5121	5.0747×10^3
FDPI-T1FDHT	9.5774	18.0999	4.3204×10^3
FDPI-IT2FDHT	9.0851	16.0875	4.0772×10^3

In Figure 12, it can be seen that compared with other methods, FDPI-IT2FDHT has the smallest overshoot and the fastest adjustment time, followed by FDPI-T1FDHT, and the worst is PI, which proves the importance of the FLS. It has been analyzed that the simple high type structure will increase the system vibration and increase the overshoot, but at the same time it will also reduce the adjustment time. Therefore, the high type structure sacrifices the overshoot in exchange for rapidity, just like the FDPI-HT simulation here. Furthermore, in Table 8, among the five methods, FDPI-IT2FDHT has the smallest evaluation index results in the no-load case, which indicates that the method performs well in all aspects. It is worth noting that the ITSE and ISE values for FDPI-HT (bolded in Table 8) are larger than those for FDPI. By analysis, this result may be caused by the excessive overshoot of FDPI-HT. However, it is its shortcomings in this respect that allow us to introduce the FLS to improve the method.

To better compare several methods, Figure 13 shows the electromagnetic torque response results in the no-load case. With the help of this figure, the superiority of the FDPI-FDHT methods, especially FDPI-IT2FDHT, can be more clearly demonstrated.

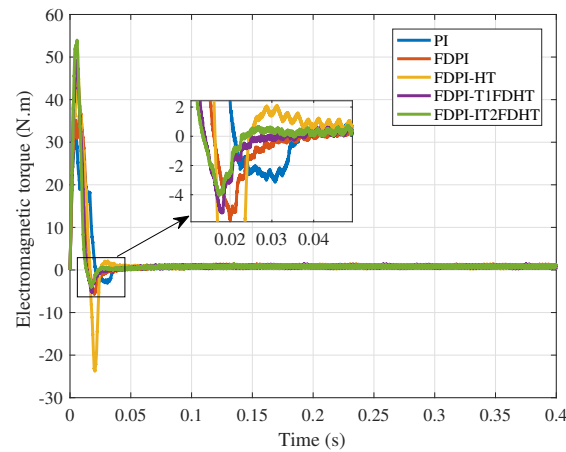


Figure 13. Electromagnetic torque response results in the no-load case.

5.3. Load Situation

In the case of load, first the motor is run in no-load mode and a load torque of 10 N · m is added at time 0.2 s. The motor speed tracking and evaluation index results of five methods under load case are, respectively, shown in Figure 14 and Table 9.

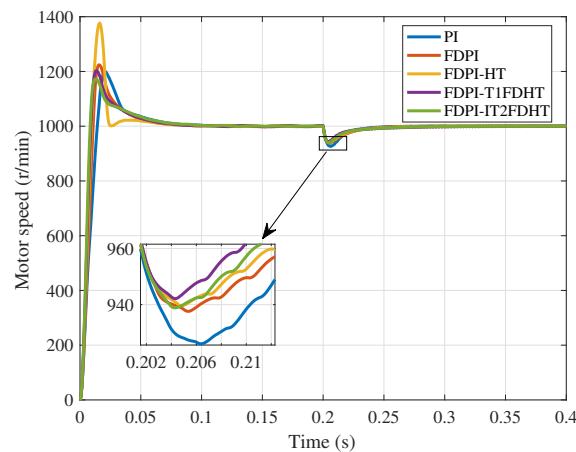


Figure 14. Motor speed tracking results under load situation.

Table 9. Evaluation indicator results under load situation.

Method	IAE	ITSE	ISE
PI	12.7659	41.2678	5.5309×10^3
FDPI	11.7122	33.4576	5.0612×10^3
FDPI-HT	10.9804	35.3746	5.1168×10^3
FDPI-T1FDHT	10.7188	25.2505	4.3542×10^3
FDPI-IT2FDHT	10.3825	24.4755	4.1169×10^3

Based on Figure 14, it can be seen that all methods oscillate once the load torque is applied, while the FDPI-FDHT (FDPI-T1FDHT and FDPI-IT2FDHT) oscillate less than their counterparts. However, we find that the oscillation amplitude of FDPI-T1FDHT is smaller than that of FDPI-IT2FDHT in the face of sudden load addition. Through analysis, the reason for this phenomenon may be that the optimization parameters of FLSs are too few. This result may be avoided if some parameters of the MFs in the FLSs are not fixed. Furthermore, in Table 9, it is clear that the FDPI-FDHT methods have better performance metric results under load, which indicates their advantage in terms of resistance to load disturbances. Again, there are some outliers here (bold font in Table 9), and the cause of these outliers is most likely the overshoot of the FDPI-HT being too high.

To add variety to the comparison, the electromagnetic torque response curves under load conditions are given in Figure 15. There is no doubt that the FDPI-IT2FDHT is the fastest to track on the given torque when the load torque is added at 0.2 s, followed by the FDPI-T1FDHT, which indicates that by adding the high type structure and FLSs, the system has shorter adjustment time, faster to reach the given speed, smoother overload when adding load suddenly, and better tracking ability to the load.

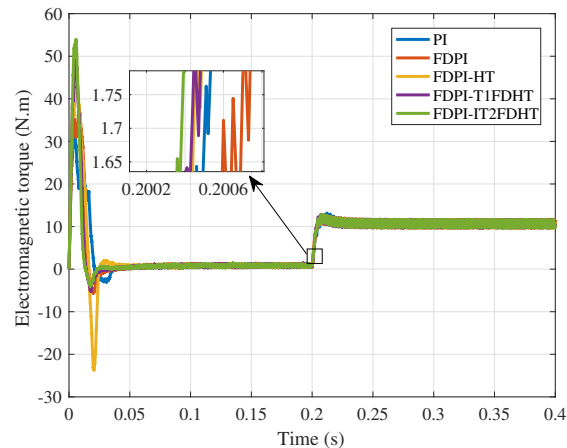


Figure 15. Electromagnetic torque response results in the load case.

Next, Figure 16 uses five subplots to show the voltage responses of u_d and u_q under different methods. Combined with the previous analysis, we can find that the voltage variation is closely related to the final speed tracking. The greater the change in voltage amplitude, the faster the speed change and the faster the speed response of the motor. As in Figure 16, FDPI-IT2FDHT improves the motor speed tracking by changing the voltage better compared to other methods.

Finally, the stator three-phase current variation curves under the five methods are compared. Since three current curves are to be shown for each method, the five subplots in Figure 17 are used below for comparison. Comparing these five sub-graphs, it can be seen that as the method is improved, the peak of the three-phase current also becomes larger and the time to enter the steady state becomes shorter. Specifically, the time to steady state for the five methods can be estimated from each enlarged graph, where PI is 0.035 s, FDPI is 0.026 s, FDPI-HT is 0.024 s, FDPI-T1FDHT is 0.022 s, and FDPI-IT2FDHT is 0.021 s.

In order to demonstrate more clearly the three-phase current variation of these five methods, a comprehensive comparison of each of the three currents is performed. Figure 18 displays the current variation of I_a , I_b , and I_c with each of the above five strategies. According to this figure, regardless of the current, the PI stator current takes the longest time to reach a sinusoidal wave at no-load start-up, adding voltage decoupling compensation shortens this time for the FDPI, and adopting a high type structure makes the time much shorter and the response speed faster. However, this rapidity is traded off by increasing the jitter before entering the steady state. In turn, FLSs are introduced to improve performance across the board. It is clear from the enlarged diagram the methods with fuzzy dynamic high type structure (FDPI-T1FDHT and FDPI-IT2FDHT) can enter the steady state faster whether under no load or with load.

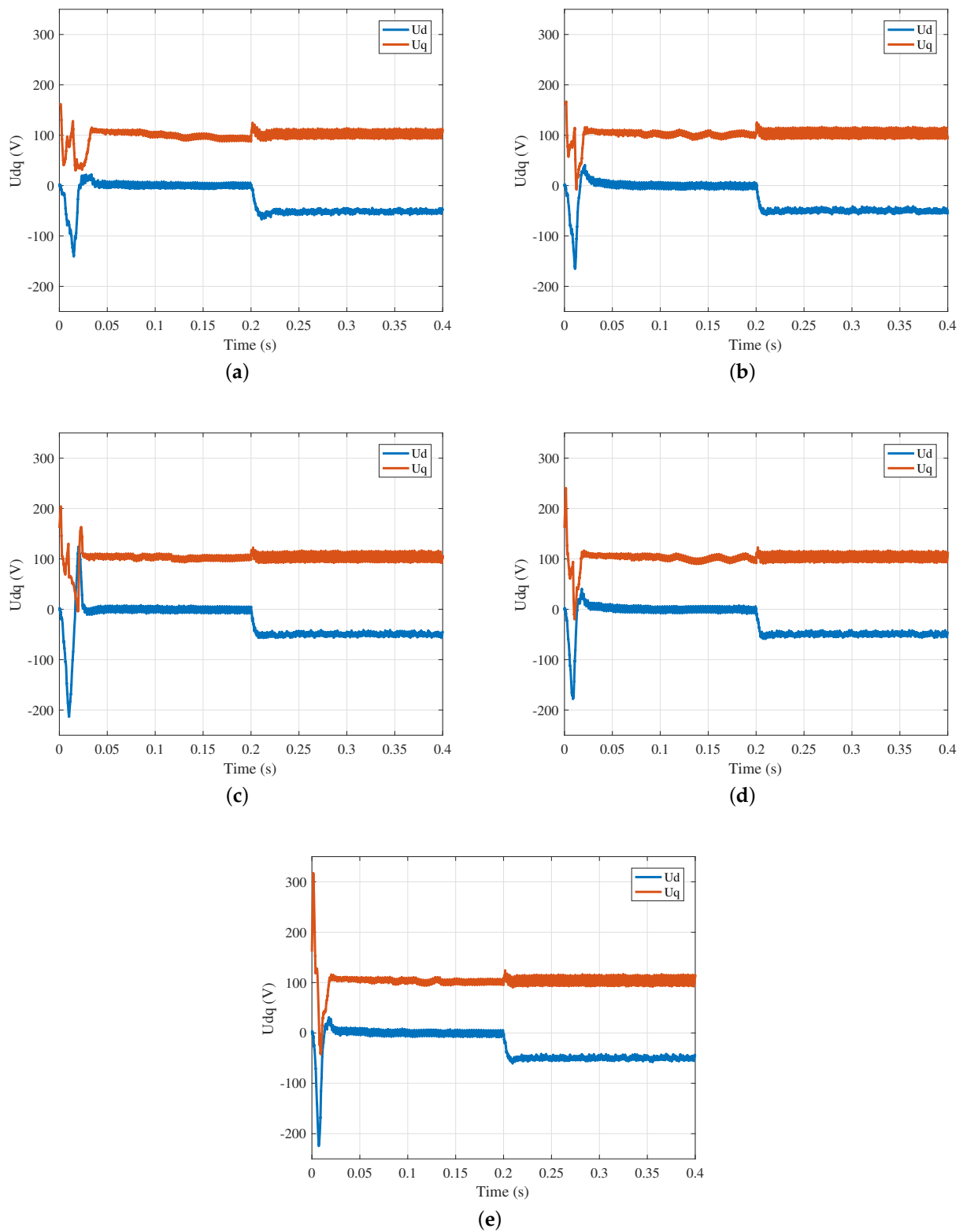


Figure 16. Voltage responses of u_d and u_q . (a) PI; (b) FDPI; (c) FDPI-HT; (d) FDPI-T1FDHT; (e) FDPI-IT2FDHT.

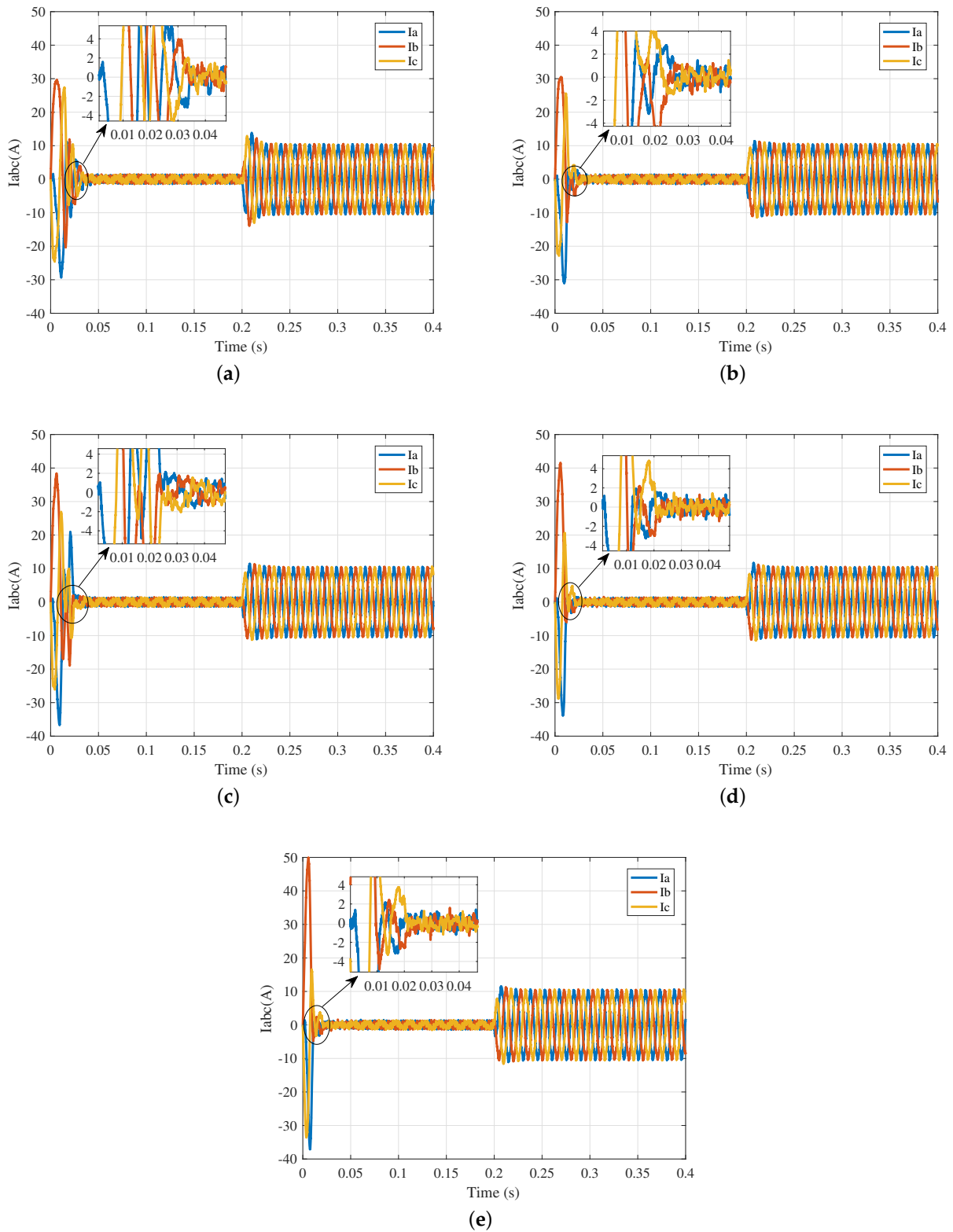


Figure 17. Three-phase current variation curves. (a) PI; (b) FDPI; (c) FDPI-HT; (d) FDPI-T1FDHT; (e) FDPI-IT2FDHT.

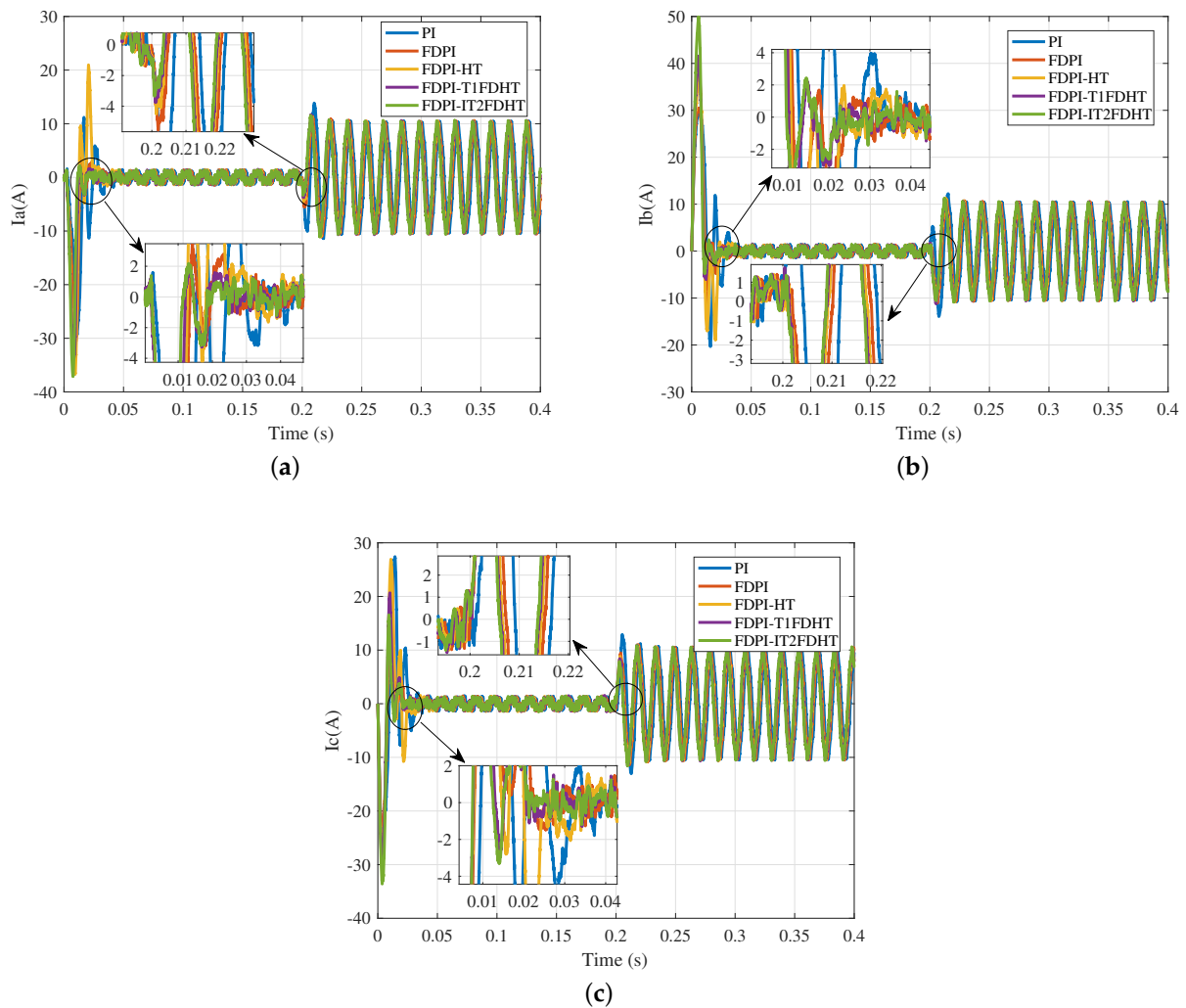


Figure 18. Current variation of I_a , I_b and I_c . (a) I_a ; (b) I_b ; (c) I_c .

6. Conclusions and Future Work

In this paper, a FDPI-IT2FDHT is proposed for PMSM to enhance the ability of dynamic response. Furthermore, to show the superiority of the designed method, PI, FDPI, FDPI-HT, and FDPI-T1FDHT are provided as well. Numerous comparative simulations suggest that FDPI with dynamic high type structure, especially FDPI-IT2FDHT, is superior to other methods in terms of dynamic characteristics and disturbance rejection, both under no-load and load conditions of the motor.

Future work will focus on improvement of FLS. Although the dynamic performance of FDPI-IT2FDHT is better than that of FDPI-T1FDHT at no load, the load oscillation of FDPI-IT2FDHT is more intense than that of FDPI-T1FDHT when a load is added, which indicates that the IT2FDHT designed in this paper is not superior to T1FDHT in all aspects and needs to be improved. Besides, we will regard experimental verification as the core of our future work.

Author Contributions: Conceptualization, X.C.; methodology, T.Z.; software, W.T.; validation, X.C. and W.T.; formal analysis, T.Z.; investigation, X.C.; resources, Y.M.; data curation, W.T.; writing—original draft preparation, W.T.; writing—review and editing, W.T.; visualization, X.C.; supervision, Y.M.; project administration, Y.M.; All authors have read and agreed to the published version of the manuscript.

Funding: This research received no external funding.

Institutional Review Board Statement: Not applicable.

Informed Consent Statement: Not applicable.

Conflicts of Interest: The authors declare no conflict of interest.

References

- Shi, Z.; Zhang, P.; Lin, J.; Ding, H. Permanent Magnet Synchronous Motor Speed Control Based on Improved Active Disturbance Rejection Control. *Actuators* **2021**, *10*, 147. [\[CrossRef\]](#)
- Sun, X.; Shi, Z.; Lei, G.; Guo, Y.; Zhu, J. Analysis and design optimization of a permanent magnet synchronous motor for a campus patrol electric vehicle. *IEEE Trans. Veh. Technol.* **2019**, *68*, 10535–10544. [\[CrossRef\]](#)
- Wang, X.; Chen, F.; Zhu, R.; Huang, X.; Sang, N.; Yang, G.; Zhang, C. A Review on Disturbance Analysis and Suppression for Permanent Magnet Linear Synchronous Motor. *Actuators* **2021**, *10*, 77. [\[CrossRef\]](#)
- Rodríguez, J.; Kennel, R.M.; Espinoza, J.R.; Trincado, M.; Silva, C.A.; Rojas, C.A. High-performance control strategies for electrical drives: An experimental assessment. *IEEE Trans. Ind. Electron.* **2011**, *59*, 812–820. [\[CrossRef\]](#)
- Adase, L.A.; Alsofyani, I.M.; Lee, K.B. Predictive torque control with simple duty-ratio regulator of PMSM for minimizing torque and flux ripples. *IEEE Access* **2019**, *8*, 2373–2381. [\[CrossRef\]](#)
- Casadei, D.; Profumo, F.; Serra, G.; Tani, A. FOC and DTC: Two viable schemes for induction motors torque control. *IEEE Trans. Power Electron.* **2002**, *17*, 779–787. [\[CrossRef\]](#)
- Gong, C.; Hu, Y.; Gao, J.; Wang, Y.; Yan, L. An improved delay-suppressed sliding-mode observer for sensorless vector-controlled PMSM. *IEEE Trans. Ind. Electron.* **2019**, *67*, 5913–5923. [\[CrossRef\]](#)
- Sant, A.V.; Khadkikar, V.; Xiao, W.; Zeineldin, H.H. Four-axis vector-controlled dual-rotor PMSM for plug-in electric vehicles. *IEEE Trans. Ind. Electron.* **2014**, *62*, 3202–3212. [\[CrossRef\]](#)
- Lakhe, R.K.; Chaoui, H.; Alzayed, M.; Liu, S. Universal Control of Permanent Magnet Synchronous Motors with Uncertain Dynamics. *Actuators* **2021**, *10*, 49. [\[CrossRef\]](#)
- Feng, G.; Lai, C.; Kar, N.C. Speed harmonic based decoupled torque ripple minimization control for permanent magnet synchronous machine with minimized loss. *IEEE Trans. Energy Convers.* **2020**, *35*, 1796–1805. [\[CrossRef\]](#)
- Moon, H.T.; Kim, H.S.; Youn, M.J. A discrete-time predictive current control for PMSM. *IEEE Trans. Power Electron.* **2003**, *18*, 464–472. [\[CrossRef\]](#)
- Guclu, R.; Gulez, K. Neural network control of seat vibrations of a non-linear full vehicle model using PMSM. *Math. Comput. Model.* **2008**, *47*, 1356–1371. [\[CrossRef\]](#)
- Xing, Q.J.; Dong, E.B.; Chen, J.; Jiang, Y.H. Dynamic high-type control for the servo system of an photoelectric theodolite. *Electron. Opt. Control* **2007**, *3*, 146–149.
- Golnaraghi, F.; Kuo, B.C. *Automatic Control Systems*; McGraw-Hill Education: New York, NY, USA, 2017.
- Tang, T.; Ma, J.; Ge, R. PID-I controller of charge coupled device-based tracking loop for fast-steering mirror. *Opt. Eng.* **2011**, *50*, 043002. [\[CrossRef\]](#)
- Papadopoulos, K.G.; Papastefanaki, E.N.; Margaris, N.I. Explicit analytical PID tuning rules for the design of type-III control loops. *IEEE Trans. Ind. Electron.* **2012**, *60*, 4650–4664. [\[CrossRef\]](#)
- Castillo, O.; Amador-Angulo, L.; Castro, J.R.; Garcia-Valdez, M. A comparative study of type-1 fuzzy logic systems, interval type-2 fuzzy logic systems and generalized type-2 fuzzy logic systems in control problems. *Inf. Sci.* **2016**, *354*, 257–274. [\[CrossRef\]](#)
- Zhao, T.; Liu, J.; Dian, S. Finite-time control for interval type-2 fuzzy time-delay systems with norm-bounded uncertainties and limited communication capacity. *Inf. Sci.* **2019**, *483*, 153–173. [\[CrossRef\]](#)
- Tong, W.; Zhao, T.; Duan, Q.; Zhang, H.; Mao, Y. Non-singleton interval type-2 fuzzy PID control for high precision electro-optical tracking system. *ISA Trans.* **2021**, in press. [\[CrossRef\]](#)
- Zhao, T.; Dian, S. State feedback control for interval type-2 fuzzy systems with time-varying delay and unreliable communication links. *IEEE Trans. Fuzzy Syst.* **2017**, *26*, 951–966. [\[CrossRef\]](#)
- Barkat, S.; Tlemçani, A.; Nouri, H. Noninteracting adaptive control of PMSM using interval type-2 fuzzy logic systems. *IEEE Trans. Fuzzy Syst.* **2011**, *19*, 925–936. [\[CrossRef\]](#)
- Chaoui, H.; Khayamy, M.; Aljarboua, A.A. Adaptive interval type-2 fuzzy logic control for PMSM drives with a modified reference frame. *IEEE Trans. Ind. Electron.* **2017**, *64*, 3786–3797. [\[CrossRef\]](#)
- Whitley, D. A genetic algorithm tutorial. *Stat. Comput.* **1994**, *4*, 65–85. [\[CrossRef\]](#)
- Marini, F.; Walczak, B. Particle swarm optimization (PSO). A tutorial. *Chemom. Intell. Lab. Syst.* **2015**, *149*, 153–165. [\[CrossRef\]](#)
- Omkar, S.; Khandelwal, R.; Ananth, T.; Naik, G.N.; Gopalakrishnan, S. Quantum behaved Particle Swarm Optimization (QPSO) for multi-objective design optimization of composite structures. *Expert Syst. Appl.* **2009**, *36*, 11312–11322. [\[CrossRef\]](#)
- Thike, R.; Pillay, P. Mathematical model of an interior pmsm with aligned magnet and reluctance torques. *IEEE Trans. Transp. Electrification* **2020**, *6*, 647–658. [\[CrossRef\]](#)
- Liu, T.T.; Tan, Y.; Wu, G.; Wang, S.m. Simulation of PMSM vector control system based on Matlab/Simulink. In Proceedings of the 2009 International Conference on Measuring Technology and Mechatronics Automation, Zhangjiajie, China, 11–12 April 2009; Volume 2, pp. 343–346.
- Zhu, H.; Xiao, X.; Li, Y. PI type dynamic decoupling control scheme for PMSM high speed operation. In Proceedings of the 2010 Twenty-Fifth Annual IEEE Applied Power Electronics Conference and Exposition (APEC), Palm Springs, CA, USA, 21–25 February 2010; pp. 1736–1739.

-
29. Xingye, G.; Chuang, L.; Yuefei, Z.; Kai, W. Analysis and dynamic decoupling control schemes for PMSM current Loop. In Proceedings of the 2016 IEEE International Conference on Aircraft Utility Systems (AUS), Beijing, China, 10–12 October 2016; pp. 570–574.
 30. Nie, M.; Tan, W.W. Towards an efficient type-reduction method for interval type-2 fuzzy logic systems. In Proceedings of the 2008 IEEE International Conference on Fuzzy Systems (IEEE World Congress on Computational Intelligence), Hong Kong, China, 1–6 June 2008; pp. 1425–1432.
 31. Leonhard, W. *Control of Electrical Drives*; Springer Science & Business Media: New York, NY, USA, 2001.